REVIEW

JAAS
www.rsc.org/jaas

Orientational information from unoriented metalloproteins by optically detected electron paramagnetic resonance

Jörg Gutschank,*[a] Dieter Suter[a] and Birgit Enkisch[b]

[a]*Universität Dortmund, Fachbereich Physik, 44221 Dortmund, Germany*
[b]*Carl Zeiss, Semiconductor Manufacturing Technologies AG, 73446 Oberkochen, Germany*

Received 15th July 2003, Accepted 24th November 2003
First published as an Advance Article on the web 11th December 2003

The electronic structure of metalloproteins can be analysed with optically detected electron paramagnetic resonance (ODEPR). This relatively young technique combines electron paramagnetic resonance (EPR) and magnetic circular dichroism (MCD) with a coherent Raman scattering experiment. It can complement conventional EPR and MCD in the deconvolution and assignment of optical transitions. Information about the relative orientation of optical and magnetic transition dipoles in metalloproteins can be extracted with considerably higher resolution than by alternative techniques such as MCD. We discuss how these features provide information about the environment of metal ions in metalloproteins.

1. Introduction

The identification and quantification of specific forms of a particular metal element is becoming increasingly important in a wide variety of fields. Metal speciation is crucial in environmental, clinical, nutritional, industrial and geochemical applications. Analytical chemists have always integrated knowledge from different scientific disciplines. We discuss here a combination of laser spectroscopy and magnetic resonance that provides very specific information about the environment of paramagnetic centers such as metal ions.

Among the spectroscopic techniques used to probe the electronic structure of paramagnetic metal ions, electron paramagnetic resonance (EPR) provides very specific information and has therefore been used extensively to probe the active centre of metalloproteins.[1] In the experiments that we discuss here, the EPR signal is detected *via* a laser beam, rather than the absorption of the microwave field. We discuss here the basics of the experiment and the information content of ODEPR spectra and show some examples of metalloproteins where the analysis of ODEPR spectra has improved our understanding of their geometrical and electronic structure.

In magnetic resonance experiments light can be used to enhance the polarisation, to influence the dynamics of the spin system and, as in the experiment described here, to improve the detection. In suitable systems, optical detection provides a number of advantages: first, optical radiation introduces an additional resonance condition, which can be used to distinguish different signal components and thereby separate the target signal from backgrounds such as impurities. Second, optical radiation can be detected with single photon sensitivity (in contrast to microwave radiation). This has made detection of single spins possible in suitable systems. A third possible use of the optical radiation is that the laser beam breaks the symmetry of isotropic samples, such as powders or frozen solutions. As we discuss in Section 5, this allows one to derive the orientation of tensorial interactions, such as electron *g*-tensors or optical anisotropy tensors from non-oriented samples.

Many different methods have been developed to exploit the advantages of optical detection for magnetic resonance.[2] In particular, magnetic resonance of electronically excited states[3] usually requires optical excitation of the sample to populate the excited states. Other techniques measure changes in the magnetic circular dichroism (MCD)[4] or other magneto-optical effects while sweeping through an EPR. The coherent ODEPR technique was first suggested by Dehmelt[5] and used on alkali vapours.[6] Bloembergen and co-workers suggested an extension to solids,[7] which was implemented by Bingham *et al.* for ruby.[8] The first biological system on which ODEPR was used for measurement was cytochrome *c*.[9]

2. Two conventional techniques

Optically detected electron paramagnetic resonance (ODEPR) combines two standard techniques for the investigation of electronic structure of paramagnetic metal centres: magnetic circular dichroism (MCD) and electron paramagnetic resonance (EPR). A basic understanding of both these methods is therefore necessary to understand ODEPR.

A. EPR

1. Basics. EPR[10] can be used to investigate the resonance frequency of a precessing magnetisation of a sample under the influence of microwave radiation and a slowly varying magnetic field.

Unpaired electrons in transition metal ions possess a magnetic moment

$$\vec{\mu} = \gamma\hbar\vec{J} = -g\mu_B\vec{J} \qquad (1)$$

where $\hbar$ is Planck's constant and γ is the gyromagnetic ratio consisting of the spectroscopic splitting factor or *g*-value g, and the Bohr magneton μ_B. The total angular momentum $\vec{J}$ (in units of $\hbar$) consists of orbital and spin contributions. The magnetisation $\vec{M}$ is the vector sum per unit volume of all magnetic moments.

Application of a magnetic field $\vec{B}_0$ exerts a torque

$$\hbar\frac{d\vec{J}}{dt} = \frac{1}{\gamma}\frac{d\vec{\mu}}{dt} = \vec{\mu}\times\vec{B}_0 \qquad (2)$$

on $\vec{\mu}$. This equation shows that the magnetic moments $\vec{\mu}$ (and therefore also $\vec{M}$) precess around $\vec{B}_0$ with the angular velocity $\omega_L = (g\ \mu_B)/(\hbar)\ B_0$, which is referred to as the Larmor frequency. The free precession is damped by relaxation and $\vec{M}$ would eventually end up aligned with $\vec{B}_0$. In order to obtain a continuous precession one has to resonantly apply energy to the system. Microwave radiation of amplitude $\vec{B}_1$ polarised perpendicular to $\vec{B}_0$ with an angular velocity $\omega_{MW} = \omega_L$ can be used to keep $\vec{M}$ at precession around $\vec{B}_0$ (Fig. 1).

DOI: 10.1039/b308090k

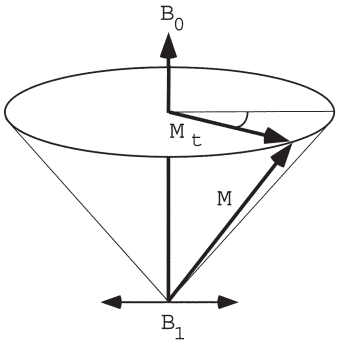

Fig. 1 The magnetisation M of a paramagnetic sample in a static magnetic field B_0 is precessing. It is kept in continuous precession at a fixed angle to B_0 by a microwave field B_1 oscillating at the Larmor frequency. EPR measures the amplitude of the component M_t transverse to the static field.

In an EPR experiment the frequency of the microwave radiation ω_{MW} is kept constant, while the strength of the magnetic field B_0 is slowly varied, in order to find the field, where the EPR resonance condition

$$\hbar\omega_{MW} = g\ \mu_B\ B_0 \qquad (3)$$

is fulfilled, so that the precession can be observed. A signal proportional to a transverse component $\vec{M}_t$ of the magnetisation (or a derivative thereof) perpendicular to the magnetic field $\vec{B}_0$ is measured as a function of B_0. The result is an absorption or dispersion curve, depending on the relative phase of excitation and detection (Fig. 2). The two signals are proportional to projections of the rotating M_t, which are 90° out of phase relative to each other: when B_0 fulfils eqn. 3, the absorption signal reaches the maximum shown in Fig. 2, while the dispersion signal goes through zero.

2. Information content. In the simplest case of a free electron, the g-factor has the value $g_f = 2.002\,32$. In all chemically interesting applications, the electron is in an atomic or molecular orbital and its magnetic moment has contributions from orbital as well as spin degrees of freedom. The g-factor deviates, therefore, from the free electron value in a way that is characteristic of its environment. In addition, the g-value depends on the orientation of the magnetic field with respect to the local environment of the unpaired electron: the g-value is then a second rank tensor with three principal values g_x, g_y and g_z,[10] where the index refers to the direction of the principal axes. In disordered systems like powders or frozen solutions, the anisotropy of the g-tensor can lead to very broad lines. The principal values of the g-tensor can then be identified by the position of the maximum and the highest and lowest g-values.

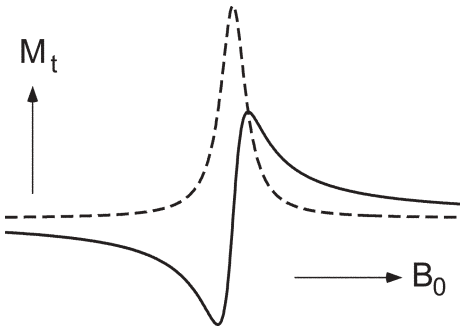

Fig. 2 Transverse magnetisation as a function of magnetic field B_0. Depending on the detection phase relative to the excitation microwave field B_1, the signal shows an absorption (broken line) or dispersion (continuous line). Conventional EPR spectrometers usually detect the derivatives of these signals.

The environment of the electron also includes nuclear spins, which couple to the electron *via* hyperfine interaction. These couplings split or broaden the EPR lines and are quantified by the hyperfine coupling constant A. Both these dependencies on the environment of the paramagnetic site make EPR spectroscopy a versatile tool for the determination of electronic as well as spatial structure.

A widely used application is the introduction of spin-labels[11] to systems which do not show EPR by themselves. g-values as well as hyperfine coupling constants are sensitive to the orientation of the label relative to the field. Further, hyperfine coupling can give information about the mobility of the spin-label and thus about the dynamics of the system.

Also in inorganic biochemistry EPR is extensively used not only to detect specific metal ions (*e.g.*, 1 μM Fe^{3+} in solution at room temperature), but also for its sensitivity to the surroundings of the ion.[12] EPR can, for instance, distinguish between 3 different types of copper centres, and some proteins contain all of them. Clarification of such a complex situation by EPR and optical spectroscopy was a milestone in inorganic biochemistry.[12] The redox states of iron Fe^{2+} and Fe^{3+} both exist in high- and low-spin states, which can clearly be distinguished by EPR, and the g-value gives further information on the surrounding ligands. Consequently EPR was often used to study haems and iron–sulfur clusters. Many other transition metal ions in proteins and enzymes are also investigated by EPR. Sometimes also organic residues in the neighbourhood of metal centres give an EPR signal, like the stable tyrosyl radical.

Variants of EPR, like electron nuclear double resonance and electron spin echo envelope modulation[13] make the identification of hyperfine interaction with the ligands (superhyperfine interaction) easier and are also often used for the investigation of paramagnetic centres and their surroundings.

B. MCD

Magnetic circular dichroism (MCD) refers to the differential absorbance ΔA of left *versus* right circularly polarised light in the presence of a magnetic field. Like optical absorption, it is a resonant phenomenon, but since it can have a positive as well as a negative sign, it often provides significantly higher resolution than the pure absorption spectrum.

MCD theory[14–17] distinguishes three terms, A, B, C, contributing to the spectrum. In paramagnetic samples like metalloproteins at low temperature the strongly temperature dependent C term usually dominates the other two. Fig. 3 illustrates the principle for an idealized spin-1/2 system: the static magnetic field in the direction of a beam of circularly polarised light lifts the degeneracy of the two opposite spin states and a population difference between them is established according to Boltzman's law. Circularly polarized light couples to only one of the two spin states, as indicated by the arrows in Fig. 3. The thermal population difference therefore implies that the polarization that couples to the lower energy state is absorbed more strongly than the opposite polarization.

In a typical MCD experiment ΔA is measured as a function

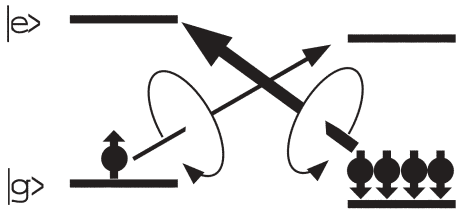

Fig. 3 C-term MCD. Optical excitation with two opposite circular polarisations from the electronic ground state $|g>$ to the excited state $|e>$ of a paramagnetic sample in a magnetic field. One polarisation finds more elctrons of the respective spin than the other.

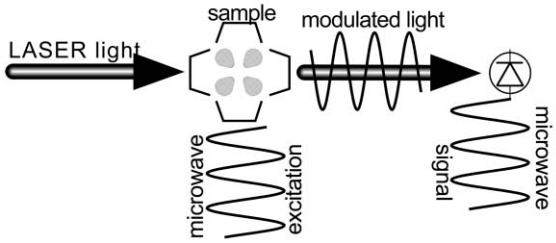

Fig. 4 The metalloprotein is irradiated with laser light and microwaves. The mixed frequency signal is detected by a fast photodiode. The output of the detector is a microwave signal.

of optical wavelength at fixed magnetic field and for several fixed temperatures. The resulting spectra are characteristic for the surrounding of a metal centre in a metalloprotein and can therefore be considered as fingerprints.

Circular dichroism can be induced not only by magnetic fields, but also by other effects that generate a net spin polarization, such as optical pumping[18] or by transverse magnetization excited by microwave irradiation, as we describe in the following section.

3. Principle of the ODEPR experiment

A. General idea

ODEPR is a coherent double resonance experiment. The metalloprotein sample is simultaneously irradiated with microwaves and laser light, which are tuned to an optical and a magnetic dipole transition in the sample. The sample is placed in a magnetic field to lift the degeneracy of the Zeeman levels. If the laser and microwave fields are both resonant with a transition in the sample, the transmitted laser beam is modulated at the microwave frequency. This modulation is picked up by a fast photodiode (see Fig. 4). The signal can be down-converted (lock-in detected) phase-sensitively with microwaves to yield the ODEPR signal.

The resulting signal depends on the optical frequency or wavelength λ as well as on the microwave frequency or the magnetic field B_0 (see Fig. 5). The signal is at a maximum when both resonance conditions are fulfilled and it decreases when either excitation becomes off-resonant.

Two complementary theoretical models exist for analysing the microscopic processes underlying this experiment, either as a modulation of the transmitted laser intensity by the precessing magnetisation or as a coherent Raman scattering process.

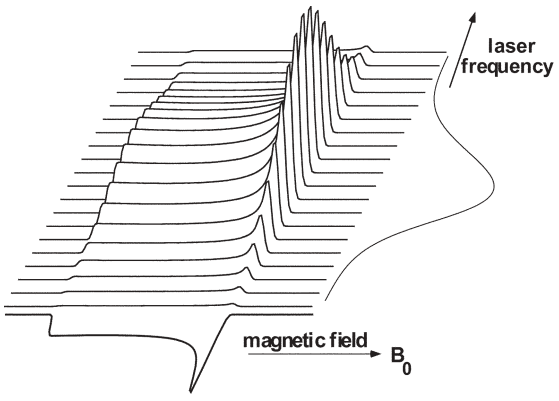

Fig. 5 The double resonant ODEPR signal depends on the laser as well as the microwave frequency. The result is a complete microwave resonance spectrum for each laser wavelength. The 2 dimensional projections on the axes are cuts through the main resonance at the peaks of the optical and the microwave transitions, respectively. (The figure was calculated from an ODEPR absorption of an axial system.)

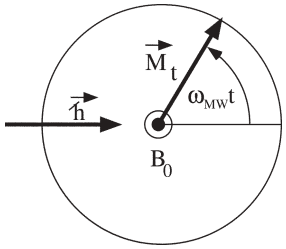

Fig. 6 Continuous wave excitation of EPR creates a component of magnetisation M_t transverse to the static magnetic field B_0 (perpendicular to the plane of drawing). The MCD of M_t is probed with circularly polarised photons with an angular momentum of $\hbar$.

B. Rotating magnetic circular dichroism

In this model, we consider a paramagnetic sample in a static magnetic field, which is continuously irradiated with resonant microwaves. The system reaches a steady state with the magnetisation precessing at the microwave frequency around the static field. As explained in Section 2A, a conventional continuous wave EPR experiment measures the component M_t of this magnetisation perpendicular to the magnetic field. In the ODEPR experiment, the same component of the magnetisation is instead probed by laser light. The conservation of angular momentum as a vector quantity during absorption implies that the absorptivity of the material depends on the instantaneous orientation of the electronic angular momentum. As is shown in Fig. 6, the precessing magnetisation modulates the circular dichroism and therefore the absorptivity of the sample at the microwave frequency. The resulting signal is therefore proportional to the EPR signal as well as to the MCD of the sample. This effect is completely analogous to MCD, where the circular dichroism due to the magnetisation parallel to the magnetic field is probed, as mentioned in Section IIB.

C. Coherent Raman scattering

The description of the ODEPR experiment as coherent Raman scattering[19] has not yet been applied to metalloproteins quantitatively. We include it here for completeness, since it is more general than the rotating MCD picture and provides additional insight into the microscopic processes that generate the observed signal.

We consider again an EPR transition of a paramagnetic sample in a magnetic field driven by a microwave field, while a laser field is applied in resonance with an optical transition. Fig. 7 shows the three quantum mechanical states that are involved in the process. The microwave field interacts with the transition between levels $|1>$ and $|2>$, while the optical field excites the transition between $|1>$ and $|3>$. The combination of the two fields creates a coherent superposition of states $|2>$ and $|3>$. (This means that the quantum mechanical wave function is a linear combination of the two separate wave functions.) Physically, the coherence in an optical transition like $|2> \leftrightarrow |3>$ represents the source of an optical field. This additional field propagates parallel to the incident laser field; its

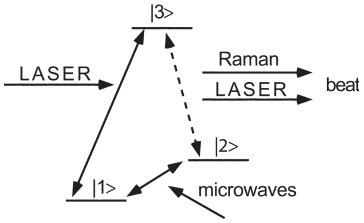

Fig. 7 Coherent Raman scattering from a 3 level system. Laser excitation creates a coherence between levels $|1>$ and $|3>$ and microwaves between $|1>$ and $|2>$. The resulting non-linear polarisation creates a Raman wave.

frequency is equal to the sum or difference of the laser and microwave frequencies. The process is known as coherent Raman scattering.[20]

Since the two optical fields propagate in the same direction, they are superimposed on the detector and create a beat signal at the difference frequency, which is equal to the frequency of the microwave field applied to the sample.

4. Experimental

The experimental setup required for ODEPR experiments is based on a conventional EPR spectrometer, augmented by a laser and some optical components for controlling the laser beam. The light is usually modulated between left and right circularly polarised with a photoelastic modulator. In order to reach the relevant wavelength range for the investigation of metalloproteins it is often necessary to use many different lasers.

The paramagnetic metalloprotein glass is placed in a cylindrical cuvette of 0.5 mm inner length and 3 mm inner diameter. The cuvette is mounted inside a microwave cavity with its microwave magnetic field B_1 parallel to the direction of propagation of the laser beam. The cavity is located inside a helium bath cryostat and has two openings for transmitting the laser beam. The 'static' (slowly swept) magnetic field B_0 of the superconducting split coil magnet is perpendicular to the propagation of the light and thus also to the microwave field B_1. The modulated light signal (or local oscillator and Raman side-band) is detected with a fast photodiode which is connected to the microwave receiver setup.

In the experiment the magnetic field B_0 is slowly swept over the resonance while the sample is irradiated with microwaves and laser light. The light after the sample carries the ODEPR signal, which is extracted in the heterodyne receiver. Details of this heterodyne receiver, which converts the optical signal to the ODEPR spectrum, have been discussed elsewhere.[21]

Finally, the signal is displayed *versus* magnetic field. After a proper calibration of the instrument,[21] the signal amplitude can be represented as the difference in absorbance ΔA or extinction coefficient $\Delta\varepsilon$ between opposite circular polarisations.[9]

5. Information content

The signal generated in this experiment depends on the optical as well as on the magnetic resonance condition. The additional resonance condition, compared with conventional EPR spectroscopy, provides a possible mechanism for distinguishing different paramagnetic centres. This is particularly important when pure samples are difficult or impossible to obtain.

Besides the chemical selectivity, the double resonance technique also provides the possibility of obtaining information about the orientation of the *g*-tensor in the molecule. The principle of this is illustrated in Fig. 8. The line shape of the ODEPR spectrum (Fig. 8 (c), (d)) differs significantly from that of the conventional EPR spectrum (Fig. 8 (e)). The difference arises from an orientational selectivity: The contribution of every molecule to the total signal is weighted with its MCD sensitivity for the direction of propagation of the laser beam. If a given molecule has the highest MCD sensitivity along the molecular *z*-axis (Fig. 8 (a), (b)), the main signal contribution (Fig. 8 (c)) arises from molecules whose *z*-axis is oriented perpendicular to the static magnetic field. For these molecules, the resonant magnetic field is determined by their g_x and g_y values. The signal intensity is then reduced around the g_z position of the spectrum, since the laser beam hardly sees MCD intensity for molecules with g_z along B_0 (Fig. 8(a)). This is in contrast to conventional EPR, where MCD sensitivity does not come into play (Fig. 8(e)).

The spectra can be calculated quantitatively by a theory that

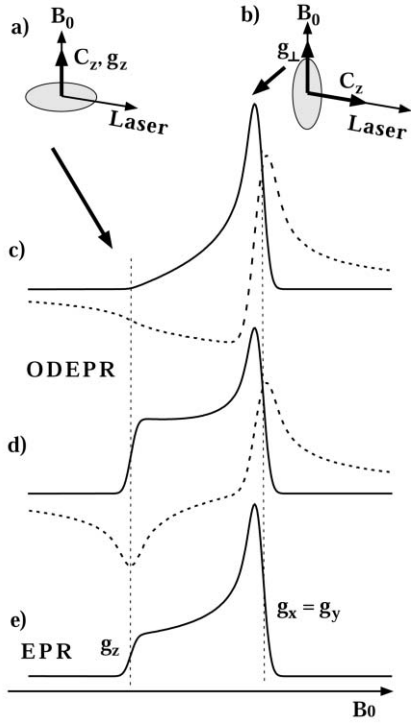

Fig. 8 ODEPR lineshapes contain orientational information. C_z represents MCD sensitivity in molecular *z*-direction and the shaded disk represents the plane of the axially symmetrical molecule. (a) Molecules with MCD sensitivity only along their *z*-axis do not contribute, when the *z*-axis is perpendicular to the laser beam. (b) They contribute strongly when the *z*-axis is parallel to the laser beam. (c) Calculated ODEPR absorption (continuous line) and dispersion (broken line) of an axially symmetrical molecule with MCD sensitivity along its *z*-axis only. (d) Calculated ODEPR when the MCD sensitivity is only perpendicular to the *z*-axis. (e) Calculated conventional EPR absorption.

combines EPR (to calculate spectral positions) and MCD (to calculate the amplitude). We discuss here only the case of an axially symmetrical system, where the difference of the extinction coefficients $\Delta\varepsilon_x$ (x indicating transverse to B_0) for circularly polarised light is[22–24]

$$\Delta\varepsilon_x \propto \int_0^{\pi/2} \sin\theta \mathrm{d}\theta T(\theta) \mathrm{f}(\theta) \left[C_Z g_Z \frac{g_\perp^2}{g^2} \sin^2\theta + C_\perp g_\perp \left(\frac{g_\perp^2}{g^2} \cos^2\theta + 1 \right) \right] \quad (4)$$

Here θ is the angle between the molecular *z*-axis and the static magnetic field, $T(\theta) = \tanh(g(\theta)\mu_B B_0/2kT)$ is the Boltzmann factor, and $f(\theta)$ describes the transverse magnetization as a function of molecular orientation, amplitude and frequency of the microwave field. $g_\perp$ and g_z are the principal values of the *g*-matrix perpendicular to and along the molecular *z*-axis and $g^2 = g_z^2 \cos^2\theta + g^2 \sin^2\theta$. $C_\perp$ and C_z are the principal values of the optical anisotropy tensor, which describes the MCD sensitivity.

To obtain the *g* and *C* values and the orientation from the experimental spectrum, we fitted the conventional as well as the optically detected EPR spectrum with the same parameter set. For the additional analysis, it is convenient to calculate the ratio $\frac{C_\perp}{C_z} = \tan\gamma$ which parametrises the direction of the optical anisotropy with respect to the *g*-tensor axis.

A comparison of ODEPR spectra measured at different optical wavelengths shows strong variations of the amplitude and lineshapes of the spectra. This variation arises because the optical anisotropy tensor *C* is a characteristic property of each optical transition. As the laser interacts with different transitions, the optical anisotropy changes and, according to eqn. 4, also the ODEPR spectrum.

To obtain the anisotropy parameters for each optical transition, we first evaluate the orientation γ as a function of the optical frequency v. We then fitted this angle together with the measured MCD $\Delta\varepsilon_z$ (z indicating parallel to B_0) to a sum of contributions i from each optical transition at position p_i with width w_i

$$\Delta\varepsilon_z(v) = \sum_i \Delta\varepsilon_{zi} e^{-(v-p_i)^2/2w_i^2} \quad (5)$$

and the orientation angles

$$\gamma(v) = \arctan\left(\frac{\sum_i C_{\perp i} e^{-(v-p_i)^2/2w_i^2}}{\sum_i C_{zi} e^{-(v-p_i)^2/2w_i^2}}\right) \quad (6)$$

6. Examples

A. Azurin, low *g*-value anisotropy

We illustrate the procedure of extracting the orientational information with the example of *Pseudomonas aeruginosa* azurin.[24] The conventional EPR spectra of azurin have the typical shape of an axially symmetrical system as shown in Fig. 9 (a). The spectrum can be fitted with the following g-values, $g_z = 2.26$ and $g_\perp = 2.045$, the hyperfine coupling constants $A_z = 172$ MHz, $A_\perp = 27$ MHz, and the EPR linewidth $\sigma_{EPR} = 55$ MHz.

The corresponding ODEPR spectra (see Fig. 9) are dispersion phase spectra, since the absorption (*i.e.*, in phase) component of the ODEPR signal is strongly saturated under the experimental parameters typically used in these experiments ($T = 1.8$ K, microwave power = 100 mW). This behaviour is exactly analogous to conventional EPR, where the absorption phase of inhomogeneously broadened lines saturates much faster than the dispersion component.[25]

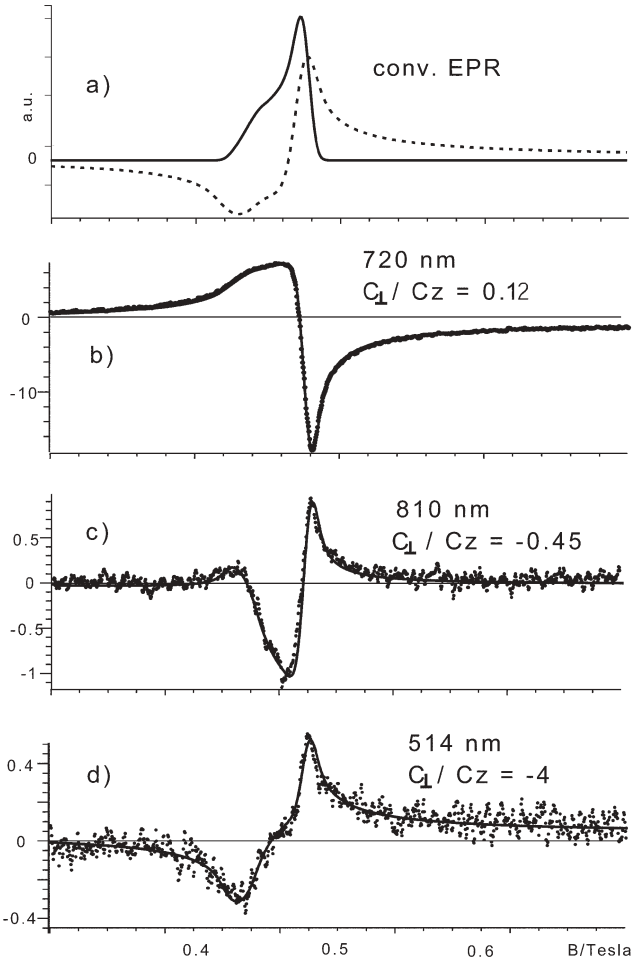

Fig. 9 (a) Simulation of conventional EPR absorption (continuous line) and dispersion (broken line). (b)–(d) Dispersion type ODEPR spectra of azurin at different optical wavelengths in units of $\Delta\varepsilon$ 10^{-3} M^{-1} cm^{-1} (broken line) and fit curves (continuous line).[24]

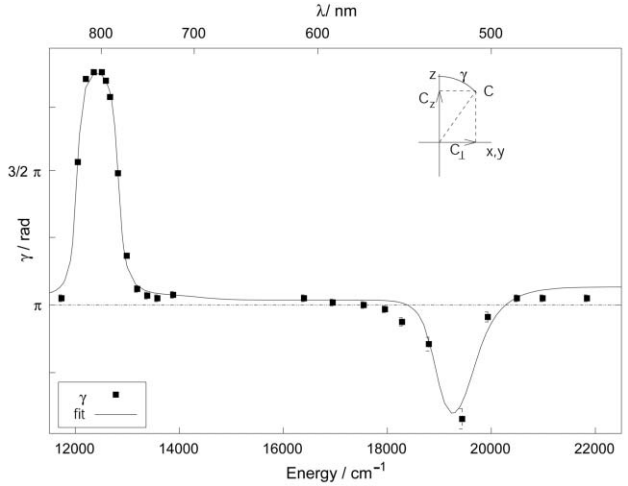

Fig. 10 Variation of the orientational angle γ with the laser wavelength. Filled squares represent experimental data, the continuous line the theory. The inset shows the definition of the orientational angle γ in the molecular coordinate system.

A comparison of the ODEPR spectra in Fig. 9 shows that the lineshape varies significantly with the laser wavelength. This variation indicates that different optical transitions are involved, and that the optical anisotropy coefficients are different for these transitions. Fitting the ODEPR spectra with eqn. 4, the orientation angle $\gamma = \arctan\frac{C_\perp}{C_z}$ can be determined for each wavelength. Over a large wavelength range, the angle is close to $\gamma = \pi$, indicating that the optical anisotropy reaches a maximum for light propagating parallel to the z-axis of the g-tensor (*i.e.*, molecular symmetry axis) and that the MCD is negative. Close to 800 nm, the MCD becomes positive ($\gamma \approx 2\pi$), and in the region close to 520 nm the angle reaches $\gamma = \pi/2$.

This variation is a strong indication of an underlying band structure. To determine this band structure, we fitted the data, together with the MCD spectrum, as discussed in Section 5, using eqn. 6 to obtain the parameters for the different optical transitions. The resulting fit, shown in Figs. 10 and 11, shows that the MCD as well as the ODEPR data can be fitted quite well with a common set of parameters. The six optical transitions determined from this fit can be associated with three ligand field and three charge transfer transitions of azurin

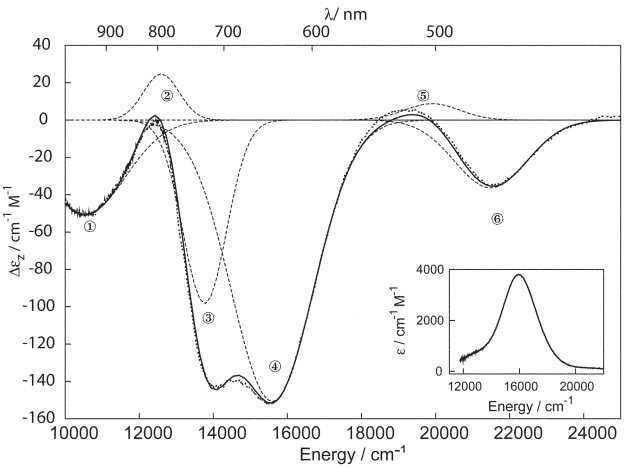

Fig. 11 MCD spectrum of azurin (continuous line) and its decomposition in six Gaussian bands (dotted lines).

Table 1 Optical transitions in azurin and their polarisation. The exact polarisation is given by the orientation angle $\gamma = \arctan(C_\perp/C_z)$. The numbers of the bands correspond to those in Fig. 11 (see Boerger *et al.*[24] for details)

Band	Energy/cm^{-1}	Transition	Main polarisation	γ
1	10 542 ± 50	Ligand field $d_{x^2-y^2}$ to d_{xy}	$-C_z$	1.03π ± 0.01π
2	12 594 ± 110	Ligand field d_{xz} to d_{xy}	$+C_z$	1.95π ± 0.01π
3	13 766 ± 75	Ligand field d_{yz} to d_{xy}	$-C_z$	1.05π ± 0.02π
4	15 592 ± 20	Charge transfer sulfur cysteine π to d_{xy}	$-C_z$	1.02π ± 0.01π
5	19 907 ± 200	Charge transfer d_{xy} to pseudo-σ	$+C_\perp$ and $+C_z$	0.25π ± 0.11π
6	21 490 ± 200	Charge transfer nitrogen histidine to d_{xy}	$-C_z$	1.07π ± 0.02π

(for a detailed discussion see ref. 24). Since the orientation of the *g*-matrix within the molecule was known from the work of Penfield,[26] the results could be related to an absolute, molecule fixed coordinate system, which was chosen with its *z*-axis close to the copper to methionine direction and its *x*-axis along the copper to cysteine direction of azurin. The resulting transitions and their polarisations are summarised in Table 1.

The example of ODEPR on azurin demonstrates the power of the method in extracting orientational information from an unoriented metalloprotein, in which the polarisations of the optical transitions were unknown before. Especially in a blue copper protein with small *g*-value anisotropy, such an assignment is hardly feasible with conventional methods such as MCD.[27]

B. Cytochrome *c* as a rhombic test system

Cytochrome *c* is a low spin ferric haem system with relatively small *g*-anisotropy. This system was the first biological sample to which the ODEPR technique was applied.[9]

From the rotating MCD model explained in Section 3B, we expect proportionality of the ODEPR signal to MCD, as well as to EPR. The proportionality to MCD was experimentally demonstrated on *Pseudomonas aeruginosa* cytochrome c551 by comparing MCD and ODEPR data of the same sample.[9] Since ODEPR measures the transverse magnetisation M_{xy}, rather than the longitudinal magnetisation M_z, the proportionality factor between ODEPR and MCD was estimated from $\frac{M_{xy}}{M_z} = \omega_{\mathrm{Rabi}} T_2$, where ω_{Rabi} is the Rabi frequency and T_2 is the phase memory time. This relation follows from the description of EPR with the Bloch equations.

The ODEPR lineshapes can be calculated quantitatively with the rotating MCD model discussed above.[23] Since the cytochrome system is not axially symmetric, the absorption of this system is not determined by eqn. 4 above, but by the more general expression eqn. 15 from Bingham *et al.*.[23] Further, the spectral lineshape indicated a distribution of *g*-values, which reflects the distribution of molecular conformations in the glass. The ODEPR dispersion spectrum of this sample, measured at a wavelength of 588 nm, can be fitted well with MCD sensitivity solely along the *z*-axis of the molecule, *i.e.*, perpendicular to the haem plane. This means that the electrons involved in the electric dipole transition move in the haem plane.

C. Rubredoxin, a high-spin system

The first high spin system to which ODEPR was applied was oxidised rubredoxin from *Clostridium pasteurianum*.[28] This electron transfer protein contains a single high-spin iron–sulfur cluster. The optical spectrum has 6 charge transfer bands in the visible and near UV region. To cover the most interesting part of this spectral range, different lasers with wavelengths between 459 nm and 560 nm were used.

The EPR spectrum of rubredoxin (conventional and ODEPR) can be explained with a zero field splitting of $D = +46.3$ GHz and a strong rhombic distortion of $E/D = 0.25$, where E is the axial and D the rhombic coefficient. The spectra showed significant deviations from the ideal spectrum expected for these parameters, which can be explained as E/D strain, *i.e.*, a statistical distribution around the mean value of 0.25. This result indicates that the protein conformation is quite variable even in the frozen solution.

The strong variation of the ODEPR lineshape with the optical excitation wavelength allowed us to identify four optical transitions in the wavelength range covered by our measurements. As in the low-spin cases, we used a simultaneous fit of the ODEPR and MCD spectra with a single parameter set. Fig. 12 shows the MCD of rubredoxin and its decomposition into the four relevant optical transitions. These results are in agreement with earlier MCD measurements by Oganesyan *et al.*[29]

Even though optical and EPR experiments had already provided most of the relevant parameters in rubredoxin, details like the orientation of the optical and magnetic tensors had remained elusive. With the combination of ODEPR and conventional EPR it was possible to find the positive sign of the zero field Hamiltonian. Further, the orientation of the *g*-tensor could be identified and the orientation of the optical symmetry axis was found to be along the direction of largest *g*-value (perpendicular to the plane of the drawing, inset in Fig. 12).

7. Conclusions

Coherent Raman detected ODEPR is a powerful method to extract orientational information from unoriented metalloproteins. It complements EPR and MCD in the elucidation of electronic structure. As a double resonance method, it correlates the magnetic and optical information. A particularly important result of this is that it can provide orientational information from isotropic samples such as frozen solutions. These possibilities have been demonstrated with the application to several metalloprotein samples with rather different parameters, such as axial and rhombic site geometry as well as high- and low-spin systems.

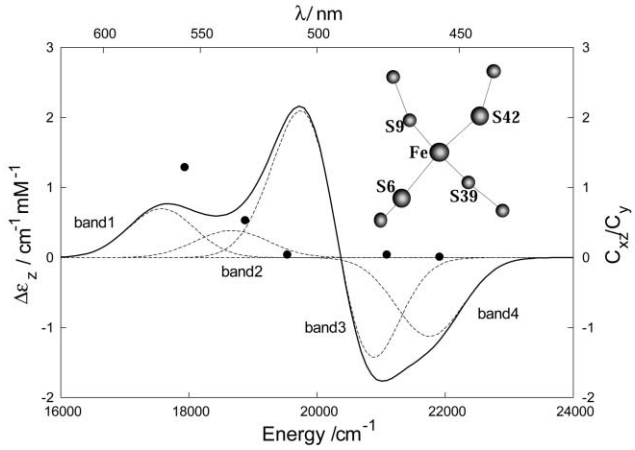

Fig. 12 MCD spectrum (solid line, left hand scale) of Rubredoxin with the four bands (dotted lines). The ratio of C_{xy}/C_y from ODEPR is indicated with dots (right hand scale). The inset shows the active site of rubredoxin, with the iron centre and the 4 sulfurs around (the pseudo-S_4-axis is perpendicular to the plane of drawing).[28]

We have developed two complementary theoretical models to describe the underlying microscopic processes. The rotating MCD theory is well developed for low spin systems and can also be used for well separated Kramers doublets in high spin systems. For more exotic cases a theory in the coherent Raman picture is available. So far, the coherent Raman theory has been quantitatively compared to experimental data only for a ruby crystal, rather than metalloproteins.

We hope to introduce the method to a broader audience concerned with the investigation of the environment of metal centres in biology.

Acknowledgements

We gratefully acknowledge contributions from S. J. Bingham, M. O. Schweika-Kresimon and A. J. Thomson, and financial support by the *Deutsche Forschungsgemeinschaft*.

References

1 G. Palmer, in *Advances in Inorganic Biochemistry*, Elsevier, Amsterdam, 1980, vol.2.
2 *Triplet State ODMR Spectroscopy*, ed. R. H. Clarke, John Wiley, New York, 1982.
3 R. H. Clarke, *Magn. Reson. Rev.*, 1973, **2**, 1.
4 C. P. Barrett, J. Peterson, C. Greenwood and A. J. Thomson, *J. Am. Chem. Soc.*, 1986, **108**, 3170.
5 H. G. Dehmelt, *Phys. Rev.*, 1957, **105**, 1924.
6 E. W. Bell and A. L. Bloom, *Phys. Rev.*, 1957, **107**, 1559.
7 N. Bloembergen, P. S. Pershan and L. R. Wilcox, *Phys. Rev.*, 1960, **120**, 2014.
8 S. J. Bingham, D. Suter, A. Schweiger and A. J. Thomson, *Phys. Lett.*, 1997, **266**, 543.
9 B. Börger, S. J. Bingham, J. Gutschank, M. O. Schweika and D. Suter, *J. Chem. Phys.*, 1999, **111**, 8565.
10 A. Abragam and B. Bleaney, *Electron Paramagnetic Resonance of Transition Ions*, Oxford University Press, London, 1970.
11 *Spin Labeling. Theory and Applications*, ed. L. J. Berliner, Academic Press, New York, 1976.
12 S. J. Lippard and J. M. Berg, *Principles of Bioinorganic Chemistry*, University Science Books, Mill Valley, 1994.
13 J. R. Pilbrow, *Transition Ion Electron Paramagnetic Resonance*, Clarendon Press, Oxford, 1990.
14 S. B. Piepho and P. N. Schatz, *Group Theory in Spectroscopy with Applications to Magnetic Circular Dichroism*, John Wiley, New York, 1983.
15 P. J. Stephens, *Adv. Chem. Phys.*, 1976, **35**, 197.
16 J. C. Sutherland, *Methods Enzymol.*, 1995, **246**, 110.
17 A. J. Thomson, M. R. Cheesman and S. J. George, *Methods Enzymol.*, 1993, **226**, 199.
18 R. Bernheim, *Optical Pumping. An Introduction*, Benjamin, New York, 1965.
19 M. O. Schweika-Kresimon, J. Gutschank and D. Suter, *Phys Rev. A*, 2002, **66**, 43816.
20 J. A. Giordmaine and W. Kaiser, *Phys Rev.*, 1966, **144**, 676–688.
21 S. J. Bingham, B. Börger, D. Suter and A. J. Thomson, *Rev. Sci. Instrum.*, 1998, **69**, 3403.
22 S. J. Bingham, B. Börger, J. Gutschank, D. Suter and A. J. Thomson, *J. Biol. Inorg. Chem.*, 2000, **5**, 30.
23 S. J. Bingham, J. Gutschank, B. Börger, D. Suter and A. J. Thomson, *J. Chem. Phys.*, 2000, **113**, 4331.
24 B. Börger, J. Gutschank, D. Suter, A. J. Thomson and S. J. Bingham, *J. Am. Chem. Soc.*, 2001, **123**, 2334.
25 A. M. Portis, *Phys. Rev.*, 1953, **91**, 1071.
26 K. W. Penfield, R. R. Gay, R. S. Himmelwright, N. C. Eickman, V. A. Norris, H. C. Freeman and E. I. Solomon, *J. Am. Chem. Soc.*, 1981, **103**, 4382.
27 F. Neese and E. Solomon, *Inorg. Chem.*, 1999, **38**, 1847.
28 B. Börger and D. Suter, *J. Chem. Phys.*, 2001, **115**, 9821.
29 V. S. Oganesyan, S. J. George, M. R. Cheesman and A. J. Thomson, *J. Chem. Phys.*, 1999, **110**, 762.